A Transcriptionally Inactive ATF2 Variant Drives Melanomagenesis

Claps, Giuseppina; Cheli, Yann; Zhang, Tongwu; Scortegagna, Marzia; Lau, Eric; Kim, Hyungsoo; Qi, Jianfei; Li, Jian-Liang; James, Brian; Dzung, Andreas; Levesque, Mitchell P; Dummer, Reinhard; Hayward, Nicholas K; Bosenberg, Marcus; Brown, Kevin M; Ronai, Ze'ev A

Abstract: Melanoma is one of the most lethal cutaneous malignancies, characterized by chemoresistance and a striking propensity to metastasize. The transcription factor ATF2 elicits oncogenic activities in melanoma, and its inhibition attenuates melanoma development. Here, we show that expression of a transcriptionally inactive form of Atf2 (Atf2(Δ8,9)) promotes development of melanoma in mouse models. Atf2(Δ8,9)-driven tumors show enhanced pigmentation, immune infiltration, and metastatic propensity. Similar to mouse Atf2(Δ8,9), we have identified a transcriptionally inactive human ATF2 splice variant 5 (ATF2(SV5)) that enhances the growth and migration capacity of cultured melanoma cells and immortalized melanocytes. ATF2(SV5) expression is elevated in human melanoma specimens and is associated with poor prognosis. These findings point to an oncogenic function for ATF2 in melanoma development that appears to be independent of its transcriptional activity.

DOI: https://doi.org/10.1016/j.celrep.2016.04.072

Report

Cell Reports

A Transcriptionally Inactive ATF2 Variant Drives Melanomagenesis

Graphical Abstract

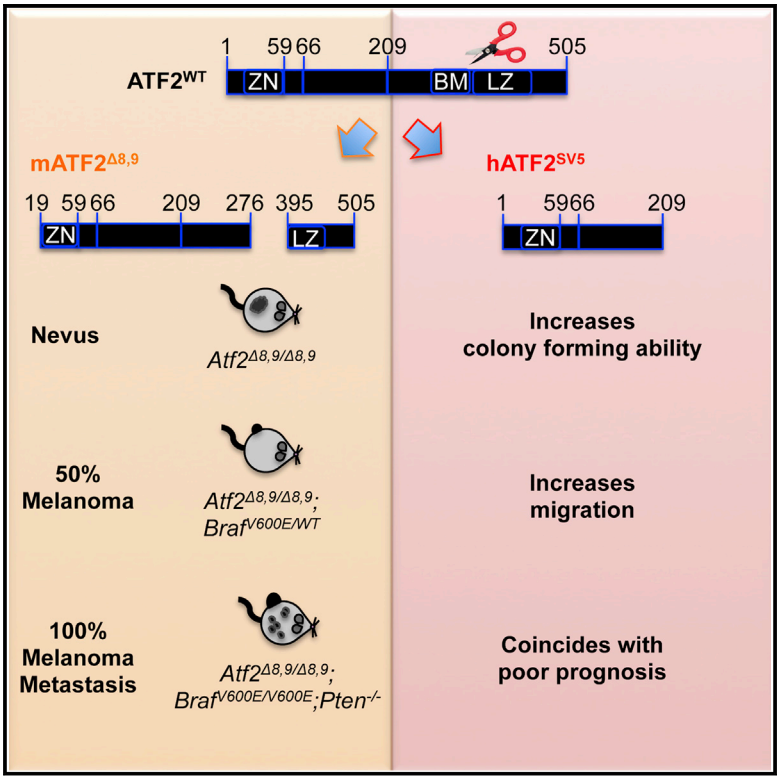

Highlights

- Transcriptionally inactive ATF2 (*Atf2*$^{\Delta 8,9}$) induces pigmentation
- *Atf2*$^{\Delta 8,9}$ induces melanoma in *Braf*^{V600E} mice
- Genes implicated in immune cell recruitment and metastasis are induced by *Atf2*$^{\Delta 8,9}$
- Human ATF2 splice variant 5 phenocopies *Atf2*$^{\Delta 8,9}$ and coincides with poor prognosis

Authors

Giuseppina Claps, Yann Cheli, Tongwu Zhang, ..., Marcus Bosenberg, Kevin M. Brown, Ze'ev A. Ronai

Correspondence

zeev@ronailab.net

In Brief

Claps et al. demonstrate that a transcriptionally inactive isoform of ATF2 lacking exons 8 and 9 is sufficient to promote melanoma in mouse models. They also identify a transcriptionally inactive human splice variant of ATF2, which resembles the mouse isoform, that is expressed in melanoma specimens and is associated with poor prognosis.

Accession Numbers

GSE79917
GSE81014

Claps et al., 2016, Cell Reports *15*, 1884–1892
May 31, 2016
http://dx.doi.org/10.1016/j.celrep.2016.04.072

OPEN ACCESS
CellPress

Cell Reports
Report

A Transcriptionally Inactive ATF2 Variant Drives Melanomagenesis

Giuseppina Claps,[1] Yann Cheli,[1] Tongwu Zhang,[2] Marzia Scortegagna,[1] Eric Lau,[1] Hyungsoo Kim,[1] Jianfei Qi,[1] Jian-Liang Li,[1] Brian James,[1] Andreas Dzung,[3] Mitchell P. Levesque,[3] Reinhard Dummer,[3] Nicholas K. Hayward,[4] Marcus Bosenberg,[5] Kevin M. Brown,[2] and Ze'ev A. Ronai[1,*]

[1]Tumor Initiation and Maintenance Program, Cancer Center, Sanford Burnham Prebys Medical Discovery Institute, La Jolla, CA 92037, USA
[2]Division of Cancer Epidemiology and Genetics, Laboratory of Translational Genomics, National Cancer Institute, Bethesda, MD 20892, USA
[3]Department of Dermatology, University of Zürich, University of Zürich Hospital, Zürich 8091, Switzerland
[4]Oncogenomics Laboratory, QIMR Berghofer Medical Research Institute, Brisbane, QLD 4006, Australia
[5]Departments of Dermatology and Pathology, Yale University School of Medicine, New Haven, CT 06520, USA
*Correspondence: zeev@ronailab.net
http://dx.doi.org/10.1016/j.celrep.2016.04.072

SUMMARY

Melanoma is one of the most lethal cutaneous malignancies, characterized by chemoresistance and a striking propensity to metastasize. The transcription factor *ATF2* elicits oncogenic activities in melanoma, and its inhibition attenuates melanoma development. Here, we show that expression of a transcriptionally inactive form of *Atf2* ($Atf2^{\Delta 8,9}$) promotes development of melanoma in mouse models. $Atf2^{\Delta 8,9}$-driven tumors show enhanced pigmentation, immune infiltration, and metastatic propensity. Similar to mouse $Atf2^{\Delta 8,9}$, we have identified a transcriptionally inactive human *ATF2* splice variant 5 ($ATF2^{SV5}$) that enhances the growth and migration capacity of cultured melanoma cells and immortalized melanocytes. $ATF2^{SV5}$ expression is elevated in human melanoma specimens and is associated with poor prognosis. These findings point to an oncogenic function for ATF2 in melanoma development that appears to be independent of its transcriptional activity.

INTRODUCTION

Melanoma is one of the most lethal cutaneous malignancies due to its metastatic propensity and resistance to therapy (Lo and Fisher, 2014). Rewired signal transduction pathways, which underlie melanoma lethality, are driven by networks of protein kinases and related transcription factors. Activating Transcription Factor 2 (ATF2) is a member of the ATF/CREB bZIP family of transcription factors, which heterodimerizes with members of the JUN and FOS transcription factor families (Lau and Ronai, 2012; Lopez-Bergami et al., 2010).

In melanoma, nuclear ATF2 expression is associated with poor prognosis and metastatic burden, whereas cytoplasmic localization correlates with sensitization of melanoma to genotoxic stress (Lau et al., 2012; Lau and Ronai, 2012) and better clinical outcome (Berger et al., 2003). Consistent with this, inhibition of ATF2 reduces melanoma growth in BRAF and NRAS mutant melanoma cell lines in culture and in xenografts (Bhoumik et al., 2002, 2004a, 2004b). Also in agreement, $Nras^{Q61K}$;$Ink4a^{-/-}$ mice selectively expressing the transcriptionally inactive form of *Atf2* ($Atf2^{\Delta 8,9}$), which lacks the DNA-binding domain and part of the leucine zipper domain (Breitwieser et al., 2007), show attenuated melanoma development (Shah et al., 2010).

In contrast, mice without melanoma susceptibility genes, but harboring $Atf2^{\Delta 8,9}$ selectively expressed in keratinocytes, display increased papilloma development when subjected to a two-stage skin carcinogenesis protocol (Bhoumik et al., 2008). Similarly, mouse embryonic fibroblasts expressing $Atf2^{\Delta 8,9}$, but lacking its homolog ATF7, show increased proliferation and formation of tumors exhibiting a JNK-ATF2-dependent gene signature in orthotopic liver cancer models (Gozdecka et al., 2014). Likewise, mutant p53 mice with deletions in the *Atf2* DNA-binding domain (amino acids 327–395) develop mammary tumors (Maekawa et al., 2008).

These observations suggest that ATF2 oncogenic or tumor suppressor function varies among tumor and tissue types depending on the landscape of genetic factors. Here, we assessed the role of ATF2 in a well-characterized genetic mouse model of Braf/Pten mutant melanoma (Dankort et al., 2009). Surprisingly, we found that transcriptionally inactive $Atf2^{\Delta 8,9}$ has a tumor-promoting effect in *Braf* mutant melanocytes, which is enhanced in *Braf*/*Pten* mutant animals.

RESULTS

$Atf2^{\Delta 8,9}$ Accelerates Melanoma Development and Metastasis Formation in $Braf^{V600E/V600E}$;$Pten^{-/-}$ Mice

To assess ATF2 function in BRAF mutant melanoma, we crossed mice expressing a transcriptionally inactive form of *Atf2* ($Atf2^{\Delta 8,9}$) (Shah et al., 2010) with $Braf^{WT/V600E}$;$Pten^{-/-}$ mice. The *Tyr::CreER*;$Atf2^{lox/lox}$;$Braf^{CA/CA}$;$Pten^{lox/lox}$ mice show melanocyte-specific expression of $Atf2^{\Delta 8,9/\Delta 8,9}$;$Braf^{V600E/V600E}$;$Pten^{-/-}$ following administration of 4-hydroxytamoxifen (4-HT). Cre-dependent deletion of *Atf2* exons 8 and 9 results in a protein lacking the DNA-binding domain and a portion of the leucine zipper (bZip) (Figures 1A and 1B) (Breitwieser et al., 2007). We

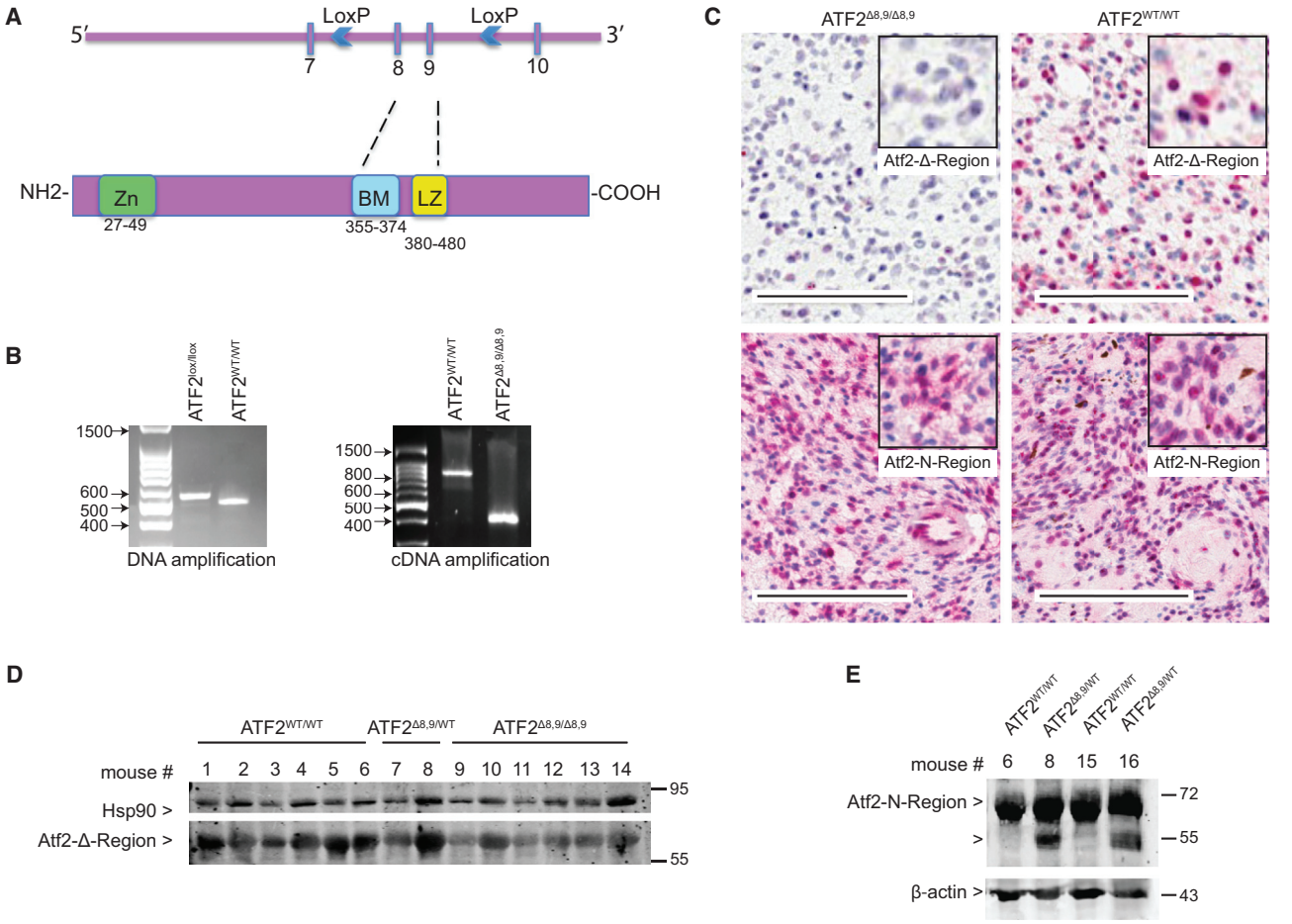

Figure 1. Generation of the *Atf2*$^{\Delta 8,9}$ Mouse Model

(A) Strategy applied to delete exons 8 and 9 of ATF2 (zinc finger: Zn; basic motif: BM; and leucine zipper: LZ). Shown is the *Atf2*^{WT} gene with the targeting exons flanked by loxP sequences.

(B) PCR analysis of DNA from *Atf2*$^{lox/lox}$ and *Atf2*$^{WT/WT}$ tail samples (left) and of cDNA obtained from *Atf2*$^{\Delta 8,9/\Delta 8,9}$ and *Atf2*$^{WT/WT}$ tumor samples (right).

(C) Immunohistochemistry (IHC) of tumor sections from *Atf2*$^{\Delta 8,9/\Delta 8,9}$ and *Atf2*$^{WT/WT}$ and animals performed with an antibody against the region deleted in ATF2$^{\Delta 8,9}$ (upper) or with an antibody to the ATF2 N-terminal region (lower). The scale bars represent 100 μm.

(D and E) Immunoblot analysis of tumor extracts from mice of the indicated genotypes using an antibody against the region deleted in ATF2$^{\Delta 8,9}$ (D) or an antibody to the ATF2 N-terminal region (E) (ATF2^{WT} = 65 kDa and ATF2$^{\Delta 8,9}$ = 55 kDa).

detected low levels of full-length ATF2, which may originate from non-tumor cells or degree of ATF2 deletion (<100% of cells; Figure 1C) in this model. Of note, the presence of full-length ATF2 in the *Atf2*$^{\Delta 8,9/\Delta 8,9}$ mice accurately reflects the co-expression of full-length and splice variant forms of ATF2 in human melanoma (see below). Further, co-expression of full-length ATF2 did not compromise the dominant activity of the ATF2$^{\Delta 8,9}$ mutant. *Atf2*$^{\Delta 8,9}$ experimental animals were monitored for expression of ATF2 variants using antibodies that recognize the ATF2 N-terminal domain or the region deleted in ATF2$^{\Delta 8,9}$ (Figures 1C–1E). Sequencing of cDNA from *Atf2*$^{\Delta 8,9}$-driven mouse tumors confirmed an in-frame transcript encoding 368 amino acids and lacking the DNA-binding domain and predicted bZip region (data not shown). This form of ATF2 retains the zinc finger and transactivation domains as well as the phosphoacceptor sites required for transcription in the N- and the DNA damage response at the C termini.

To determine the role of *Atf2*$^{\Delta 8,9}$ in melanoma development, 4-HT was administered systemically to *Atf2*$^{WT/WT}$;*Braf*$^{V600E/V600E}$;*Pten*$^{-/-}$ (n = 30) and *Atf2*$^{\Delta 8,9/\Delta 8,9}$;*Braf*$^{V600E/V600E}$;*Pten*$^{-/-}$ (n = 28) or *Atf2*$^{WT/\Delta 8,9}$;*Braf*$^{V600E/V600E}$;*Pten*$^{-/-}$ (n = 18) mice (Figure S1A, upper). 4-HT-treated *Atf2*$^{\Delta 8,9/\Delta 8,9}$ mice were more heavily pigmented than *Atf2*$^{WT/WT}$ animals (Figure 2A). Increased pigmentation was seen throughout the dermis and subcutis of *Atf2*$^{\Delta 8,9/\Delta 8,9}$ mice (n = 6) compared with *Atf2*$^{WT/WT}$ controls (n = 6), with spreading into the epidermis (Figure 2B). Despite these changes, the median survival time of the *Atf2*$^{WT/WT}$, *Atf2*$^{\Delta 8,9/\Delta 8,9}$, and *Atf2*$^{WT/\Delta 8,9}$ mice did not differ (18–19 days), possibly due to the rapid melanoma development in this model (Figure S1B).

To monitor tumor growth over a prolonged period, we administered 4-HT locally on the dorsal skin of 3-week-old *Atf2*$^{WT/WT}$;*Braf*$^{V600E/V600E}$;*Pten*$^{-/-}$ (n = 19) and *Atf2*$^{\Delta 8,9/\Delta 8,9}$;*Braf*$^{V600E/V600E}$;*Pten*$^{-/-}$ (n = 12) mice (Figure S1A, lower). *Atf2*$^{\Delta 8,9/\Delta 8,9}$ animals

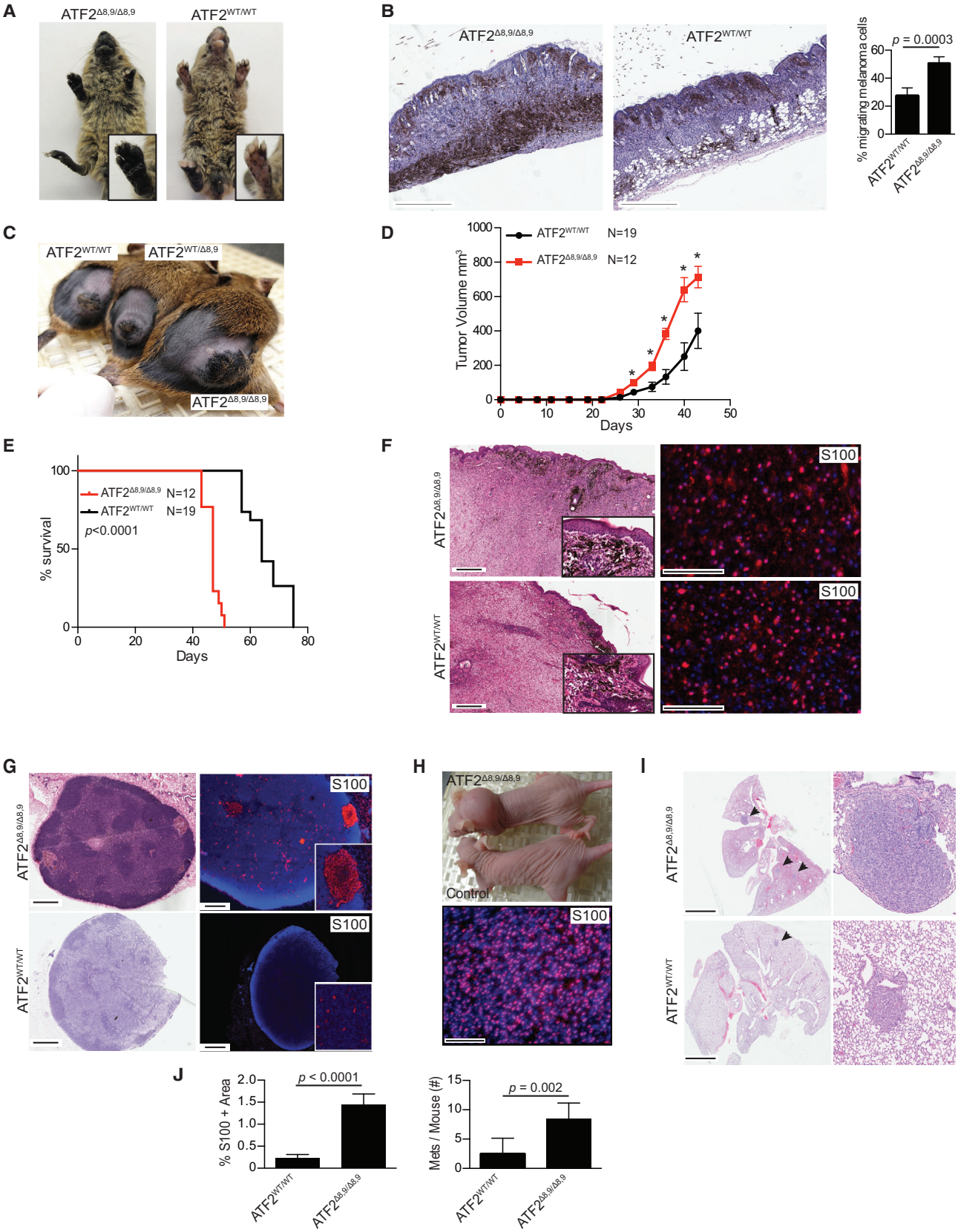

(legend on next page)

developed larger tumors (Figure 2C) that appeared earlier in control mice (Figure 2D). The median survival time of *Braf*$^{V600E/V600E}$;*Pten*$^{-/-}$ mice was decreased from 64 to 47 days by *Atf2*$^{\Delta 8,9/\Delta 8,9}$ expression (Figure 2E). The *Atf2*$^{\Delta 8,9/\Delta 8,9}$ mice had a larger number of highly pigmented cells, which were confirmed to be of melanocytic origin based on S100 immunostaining (Figure 2F). These data suggest that expression of *Atf2*$^{\Delta 8,9}$ in *Braf*$^{V600E/V600E}$;*Pten*$^{-/-}$ mice promotes melanoma development.

S100 staining revealed an increased number of metastatic melanoma cells in the lymph nodes of ATF2$^{\Delta 8,9}$ mice subjected to local 4-HT treatment compared with similarly treated ATF2^{WT} mice (Figures 2G and 2J, left). To determine whether these lesions represent metastatic melanoma, we collected lymph nodes from *Atf2*$^{\Delta 8,9/\Delta 8,9}$ and control *Atf2*$^{WT/WT}$ mice bearing tumors, which were (either the whole lymph nodes or following partial digestion; Figure S1C) transplanted into nude mice. Under both approaches, the recipient mice developed tumors, confirming that the clusters of subcapsular S100-positive cells in the lymph nodes of *Atf2*$^{\Delta 8,9/\Delta 8,9}$;*Braf*$^{V600E/V600E}$;*Pten*$^{-/-}$ mice are metastatic melanoma cells. S100 staining of tumors emerging after transplantation confirmed the presence of non-pigmented melanoma cells, as seen in the non-pigmented lymph node source (Figures 2H and S1D). In addition, the number of lesions in the lungs was higher in *Braf*$^{V600E/V600E}$;*Pten*$^{-/-}$ mice harboring *Atf2*$^{\Delta 8,9/\Delta 8,9}$ versus *Atf2*$^{WT/WT}$ (Figures 2I and 2J, right). These observations point to the higher metastatic propensity of ATF2$^{\Delta 8,9}$ expressing melanocytes.

Atf2$^{\Delta 8,9}$ Exerts Oncogenic Activity in *Braf*$^{V600E/V600E}$;*Pten*$^{-/-}$ Melanoma

As the finding that a transcriptionally inactive form accelerates melanoma development and promotes metastasis in the *Braf*$^{V600E/V600E}$;*Pten*$^{-/-}$ murine melanoma model was unanticipated, we set to further characterize the activities of ATF2$^{\Delta 8,9}$ in BRAF mutant melanoma.

Using the congenic YUMM1.3 melanoma cell line, which was derived from a C57BL/6 *Braf*$^{WT/V600E}$;*Pten*$^{-/-}$;*Cdkn2a*$^{-/-}$ melanoma, we compared the effects of ATF2$^{\Delta 8,9}$ expression versus small hairpin (sh)RNA-mediated knockdown (KD) of endogenous ATF2. ATF2 shRNA-expressing cells formed fewer colonies than control YUMM1.3 cells (Figures 3A and S2A–S2C), consistent with earlier studies. In contrast, ATF2$^{\Delta 8,9}$ overexpression (OE) conferred a growth advantage on YUMM1.3 cells compared with ATF2^{WT} OE (Figures 3A and S2C). Similarly, ATF2 KD attenuated and ATF2$^{\Delta 8,9}$ OE increased migration of YUMM1.3 compared with their respective controls (Figures 3B and S2C). These observations are consistent with observations made in the ATF2$^{\Delta 8,9}$ mouse model.

Gene expression profiles of tumor samples from *Atf2*$^{\Delta 8,9/\Delta 8,9}$;*Braf*$^{V600E/V600E}$;*Pten*$^{-/-}$ and *Atf2*$^{WT/WT}$;*Braf*$^{V600E/V600E}$;*Pten*$^{-/-}$ mice identified 579 genes (655 probes) that were significantly differentially expressed (Table S1). Of these, 305 genes (337 probes) were upregulated and 274 gene (318 probes) were downregulated in *Atf2*$^{\Delta 8,9/\Delta 8,9}$ tumors compared with *Atf2*$^{WT/WT}$ tumors. Genes with significant FDR-adjusted p values were subjected to Ingenuity Pathway Analysis (IPA), which revealed immune receptor and response signaling, angiogenesis, and ROS/NOS signaling components to be among those most significantly altered in the ATF2$^{\Delta 8,9}$ tumors (Figure 3C; Table S2A). The respective functional networks predicted to be activated in *Atf2*$^{\Delta 8,9/\Delta 8,9}$-expressing tumors included pigmentation, inflammation, cell motility, and invasion (Table S2B). Representative genes, including S100A8, implicated in macrophage recruitment; *Mmp3*, *Mmp9*, and *Ccr7*, implicated in tumor cell invasion and metastasis; *Cxcl9* and *Ctla4*; and *Mitf* and related pigmentation genes were confirmed for their increased expression in *Atf2*$^{\Delta 8,9/\Delta 8,9}$ tumors (Figure S2D). *Atf2*$^{\Delta 8,9}$-driven melanoma indeed exhibits greater pigmentation (Figure 2F), markedly increased immune cell infiltration (CD45^{+} and F4/80^{+}; Figures S2E and S2F), and an enhanced propensity to metastasize (Figures 2G–2I), compared to *Atf2*^{WT} melanoma.

Mouse *Atf2*$^{\Delta 8,9}$ Structurally Resembles an *ATF2* Splice Variant Expressed in Human Melanoma

To determine whether human tumors express an analogous form of ATF2, we interrogated RNA-sequencing (seq) expression data obtained from >70 melanoma lines and three melanocyte lines (Dutton-Regester et al., 2012). Of the four reported human ATF2 isoforms (http://www.ncbi.nlm.nih.gov/gene/1386), we confirmed the expression of three in the human melanoma set

Figure 2. Systemic or Local Induction of *Atf2*$^{\Delta 8,9}$ Expression in Melanocytes Accelerates Melanoma Development and Metastasis in *Braf*$^{V600E/V600E}$;*Pten*$^{-/-}$ Mice

(A) Representative images of *Atf2*$^{WT/WT}$ and *Atf2*$^{\Delta 8,9/\Delta 8,9}$ animals 18 days following perinatal 4-HT administration.

(B) H&E staining analysis of skin from *Atf2*$^{WT/WT}$ and *Atf2*$^{\Delta 8,9/\Delta 8,9}$ animals 18 days following perinatal 4-HT administration (left) and quantification of the percentage of migrating melanoma cells in the skin (right). The data are the mean ± SEM of skin samples from n = 6 mice per genotype. The scale bars represent 500 μm.

(C) Representative picture of *Atf2*$^{WT/WT}$, *Atf2*$^{\Delta 8,9/\Delta 8,9}$, and *Atf2*$^{WT/\Delta 8,9}$ animals 40 days following local 4-HT administration.

(D) Growth curves for tumors from *Atf2*$^{WT/WT}$ (n = 19) and *Atf2*$^{\Delta 8,9/\Delta 8,9}$ (n = 12) mice from six different litters following local administration of 4-HT. The data are the mean ± SEM (p value was calculated by two-tailed unpaired t test).

(E) Kaplan-Meier survival curves for *Atf2*$^{WT/WT}$ (n = 19) and *Atf2*$^{\Delta 8,9/\Delta 8,9}$ (n = 12) mice following local administration of 4-HT. The mice from six different litters were analyzed ($p < 0.0001$ by log rank [Mantel-Cox] test).

(F) H&E analysis (left) and S100 immunostaining (right) of tumors from *Atf2*$^{WT/WT}$ and *Atf2*$^{\Delta 8,9/\Delta 8,9}$ mice following local 4-HT administration. The scale bars represent 400 μm (H&E) and 100 μm (immunofluorescence [IF]).

(G) H&E analysis (left) and S100 immunostaining (right) of lymph nodes from *Atf2*$^{WT/WT}$ and *Atf2*$^{\Delta 8,9/\Delta 8,9}$ mice following local 4-HT administration. The scale bars represent 500 μm (H&E) and 600 μm (IF).

(H) (Upper) Representative images of nude mice transplanted with whole lymph nodes from *Atf2*$^{\Delta 8,9/8,9}$ or *Atf2*$^{WT/WT}$ (control) animals. S100 immunostaining of *Atf2*$^{\Delta 8,9/8,9}$ tumors from lymph node-transplanted nude mice is shown (lower). The scale bar represents 100 μm.

(I) H&E analysis of lungs from *Atf2*$^{\Delta 8,9/8,9}$ and *Atf2*$^{WT/WT}$ mice following local 4-HT administration. The scale bars represent 3 mm.

(J) Quantification of metastasis in lymph nodes (left) and lungs (right) in ATF2$^{WT/WT}$ (*Atf2*$^{WT/WT}$;*Braf*$^{V600E/V600E}$;*Pten*$^{-/-}$) and ATF2$^{\Delta 8,9/\Delta 8,9}$ (*Atf2*$^{\Delta 8,9/\Delta 8,9}$;*Braf*$^{V600E/V600E}$;*Pten*$^{-/-}$) mice. The data are the mean ± SEM of n = 4 mice ($p < 0.0001$ and $p = 0.002$ by two-tailed unpaired t test). See also Figure S1.

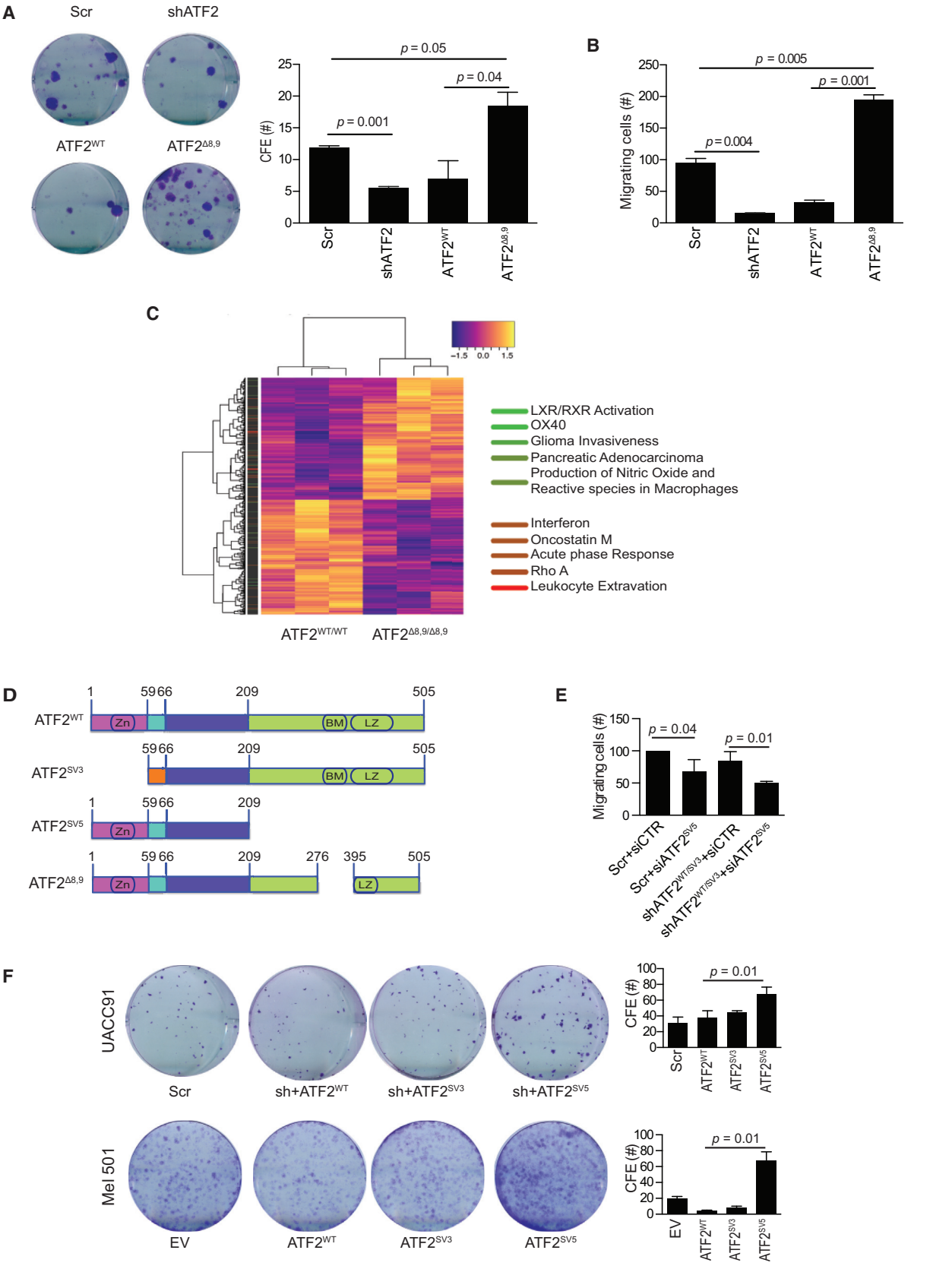

(legend on next page)

using a mixture of isoforms (MISO) analysis (Figure S3A) (Katz et al., 2010; Wang et al., 2008) and in a smaller panel of 23 melanoma cell lines by quantitative (q)PCR (Figure S3B). These analyses verified the expression of full-length ATF2 (isoform 1; $ATF2^{WT}$); isoform 3, a splice variant (SV3) that lacks the N-terminal region ($ATF2^{SV3}$); and isoform 5, a splice variant (SV5) that lacks the DNA-binding and the leucine zipper domains ($ATF2^{SV5}$) and thus partially resembles mouse $Atf2^{\Delta 8,9}$ (Figure 3D). $ATF2^{WT}$ and $ATF2^{SV3}$ are expressed at varying levels in colon, breast, and prostate tumor cells, whereas $ATF2^{SV5}$ exhibited a more selective expression (breast cancer and melanoma cells; Figure S3C).

Human $ATF2^{SV5}$ Phenocopies Mouse $Atf2^{\Delta 8,9}$ Function

To determine whether $ATF2^{SV5}$ elicits oncogenic activities similar to mouse $ATF2^{\Delta 8,9}$, we examined human UACC1113 cells, which express high levels of $ATF2^{SV5}$ in addition to $ATF2^{WT}$ and $ATF2^{SV3}$ (Figure S3B). Silencing of $ATF2^{SV5}$ in UACC1113 cells reduced their migration compared to cells in which both $ATF2^{SV3}$ and $ATF2^{WT}$ were silenced (Figures 3E and S4A). Furthermore, although colony formation by the UACC91 melanoma cell line (which does not express $ATF2^{SV5}$; Figure S3B) was reduced by silencing of endogenous *ATF2* (Figures S4B and S4C), it was rescued to a greater extent by reconstitution with $ATF2^{SV5}$ than by reconstitution with either $ATF2^{WT}$ or $ATF2^{SV3}$ (Figures 3F and S4D). Likewise, ectopic expression of $ATF2^{SV5}$ in human Mel501 cells (which do not express $ATF2^{SV5}$; Figures S3B and S4E), without silencing endogenous ATF2, also increased colony formation compared with $ATF2^{WT}$ and $ATF2^{SV3}$ (Figures 3F, S4E, and S4F). In these cells, the expression level of ectopic $ATF2^{SV5}$ was comparable to that of ectopic $ATF2^{WT}$, and both proteins were expressed at ~3-fold higher levels than the endogenous proteins (data not shown). These observations suggest that human $ATF2^{SV5}$ phenocopies mouse $ATF2^{\Delta 8,9}$.

$Atf2^{\Delta 8,9}$ Induces Nevus Formation and Promotes Melanoma in $Braf^{WT/V600E}$ Mice

The finding that $ATF2^{\Delta 8,9}$ augments melanoma development when combined with *Pten* deletion and *Braf* mutation prompted us to assess its possible role in melanomagenesis in the absence of *Pten* inactivation. Strikingly, $Atf2^{\Delta 8,9/\Delta 8,9}$;$Braf^{WT/WT}$;$Pten^{WT/WT}$ mice developed more and larger nevi than $Atf2^{WT/WT}$;$Braf^{WT/WT}$;$Pten^{WT/WT}$ mice (Figures 4A and S4G). Similarly, $Atf2^{\Delta 8,9/\Delta 8,9}$ mice had an increased number of pigmented hair follicles than $Atf2^{WT/WT}$ mice (Figures S4H and S4I).

When crossed with $Braf^{WT/V600E}$ animals, $Atf2^{\Delta 8,9/\Delta 8,9}$ mice developed melanoma within 250 days (Figures 4B–4D and S4J). Tumor penetrance was 50% for the $Atf2^{\Delta 8,9/\Delta 8,9}$ genotype, compared with 28% and 0% for the $Atf2^{WT/\Delta 8,9}$ and $Atf2^{WT/WT}$ genotype, respectively (Figure 4B). On their own, $Atf2^{\Delta 8,9}$ mice did not develop tumors, even when maintained for 250 days. Within the first 50 days, the $Atf2^{\Delta 8,9}$ mutation did not affect the pigmentation level in $Braf^{WT/WT}$;$Pten^{-/-}$ animals (data not shown). These findings identify $Atf2^{\Delta 8,9}$ as a driver of melanocyte biogenesis, highlighted by the degree of pigmentation, and demonstrate that when combined with mutant $Braf^{V600E}$, it is sufficient to induce melanoma development. The slow rate of melanoma development and progression seen in the $Atf2^{\Delta 8,9}$ animals recapitulates the time course of human melanoma (Balch et al., 2009).

To compare the activities elicited by $ATF2^{\Delta 8,9}$ and $ATF2^{SV5}$, we silenced endogenous $ATF2^{WT}$ and $ATF2^{SV3}$ in non-transformed human melanocytes (Hermes 3A [H3A]) and ectopically expressed either $ATF2^{\Delta 8,9}$ or $ATF2^{SV5}$ (Figure S4K). While silencing of ATF2 in these cells reduced colony formation (Figure S4L), consistent with earlier studies, expression of either $ATF2^{SV5}$ or $ATF2^{\Delta 8,9}$ increased H3A proliferation and migration compared with $ATF2^{WT}$ expression (Figures 4E and 4F). Moreover, H3A cells expressing $ATF2^{SV5}$ or $ATF2^{\Delta 8,9}$ and either constitutively active $BRAF^{V600E}$ or $NRAS^{Q61K}$ (Figures S4M and S4N) showed enhanced colony formation compared with cells reconstituted with $ATF2^{WT}$ (Figures 4G and 4H). Finally, migration of H3A cells was decreased to a greater degree by silencing of $ATF2^{SV5}$ compared with silencing of $ATF2^{WT/SV3}$ (Figures 4I and S4O).

RNA-seq analysis of H3A cultures identified 434 genes that were upregulated and 580 genes that were downregulated after treatment with $siATF2^{SV5}$ compared with control small interfering (si)RNA, but that were not significantly altered following $siATF2^{WT}$ treatment (Table S3). IPA analysis identified a number of pathways deregulated by $ATF2^{SV5}$ KD (Figure 4J). To validate genes that may be commonly deregulated by $ATF2^{SV5}$ and $ATF2^{\Delta 8,9}$ expression, siRNA-mediated KD of $ATF2^{SV5}$ and $ATF2^{WT/SV3}$ in the human melanoma cell lines LU1205 and C054 (Figure S4P) allowed us to assess the changes in the expression of genes identified in our expression studies (Table S3) and IPA analysis (Figure 4J). Among the genes confirmed to be altered by both ATF2 variants were *CCL4*, *CCR7*, *S100A8* (implicated in metastasis), *TIM3* (immune checkpoint), and *MITF* (Figure 4J).

IPA analyses to identify potential common mechanisms of oncogenic activities for both mouse $Atf2^{\Delta 8,9}$ and human $ATF2^{SV5}$, identified signaling and networks associated with immune cell infiltration and cell motility in both melanocytes that were subjected to $ATF2^{SV5}$ KD in H3A cells and in tumors from $Atf2^{\Delta 8,9/\Delta 8,9}$;$Braf^{V600E/V600E}$;$Pten^{-/-}$ mice (Tables S2B, S4A, and S4B).

Figure 3. Human $ATF2^{SV5}$ Phenocopies Mouse $ATF2^{\Delta 8,9}$

(A and B) Colony forming assay (A) and Transwell migration assay (B) of YUMM1.3 cells stably transduced with control vector (Scr) or vectors expressing ATF2 shRNA (shATF2), $ATF2^{WT}$, or $ATF2^{\Delta 8,9}$. The data are the mean ± SEM (p value was calculated by two-tailed unpaired t test).

(C) Heatmap showing gene expression in $ATF2^{WT/WT}$ or $ATF2^{\Delta 8,9}$ tumors. The pathways indicated on the right are deregulated by $ATF2^{\Delta 8,9}$.

(D) Schematic of three ATF2 isoforms (WT, SV3, and SV5) identified in human melanoma cell lines by MISO analysis. The mouse $ATF2^{\Delta 8,9}$ isoform is shown at the bottom.

(E) Migration assay of human melanoma UACC1113 cells transduced with control (Scr) or with a vector expressing shATF2 (targeting $ATF2^{WT}$ and $ATF2^{SV3}$, but not $ATF2^{SV5}$) and transfected with control siRNA or siRNA targeting $ATF2^{SV5}$. The data are the mean ± SD (p value was calculated by two-tailed unpaired t test).

(F) (Upper row) Colony forming UACC91 human melanoma cells transduced with control (Scr) or with vectors expressing shATF2 plus $ATF2^{WT}$, $ATF2^{SV5}$, or $ATF2^{\Delta 8,9}$. Mel501 human melanoma cells stably transduced with pLX304 (empty vector, EV) or vectors expressing $ATF2^{WT}$, $ATF2^{SV5}$, or $ATF2^{SV3}$ (lower row). The data are the mean ± SEM (p value was calculated by two-tailed unpaired t test). See also Figures S2 and S3 and Tables S1 and S2.

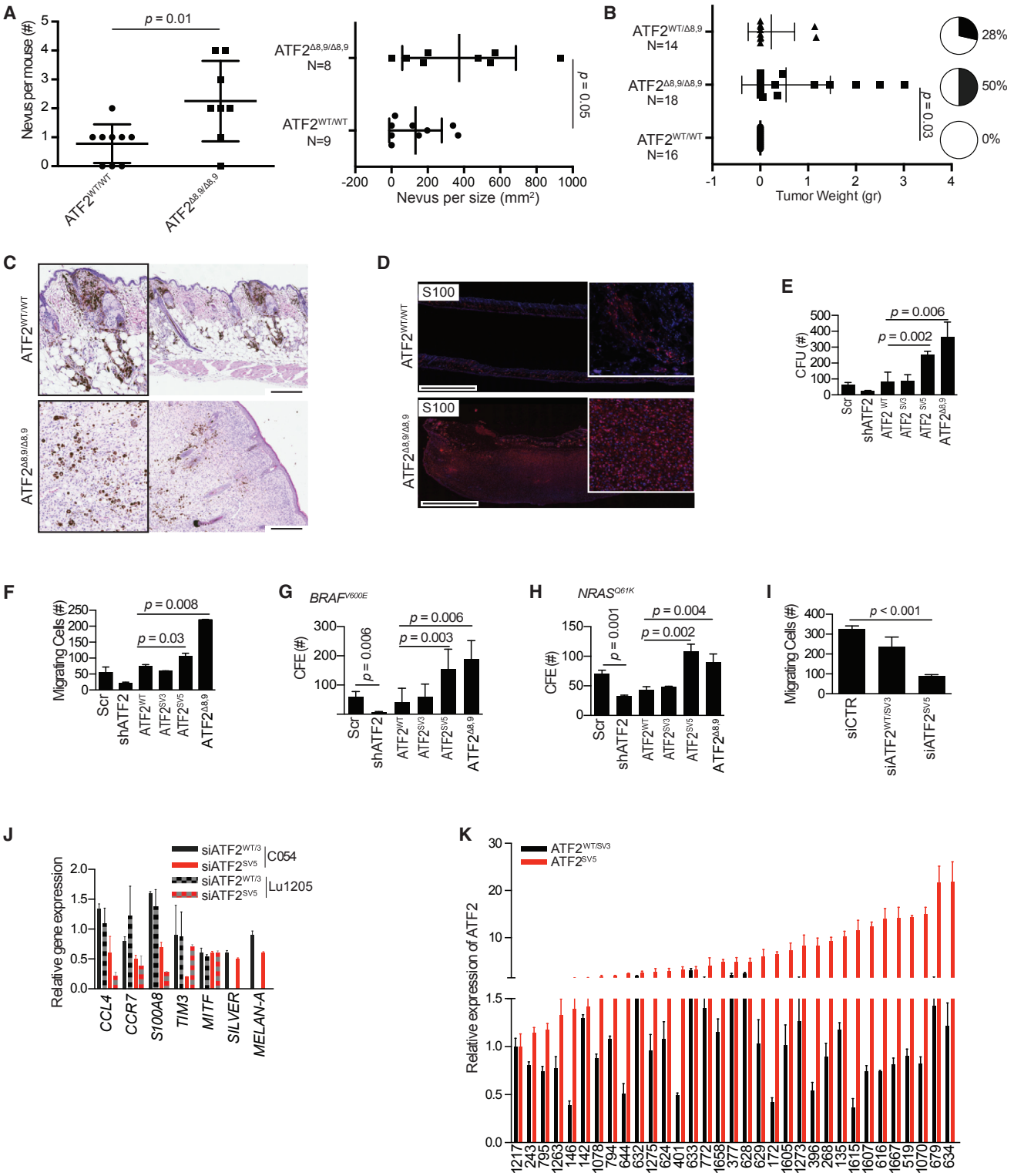

Figure 4. *Atf2*$^{\Delta 8,9}$ Expression in Melanocytes Accelerates Nevus Formation in *Braf*$^{WT/WT}$ Mice and Melanoma Development in *Braf*$^{WT/V600E}$ Mice

(A) Quantification of nevi per mouse (left) and nevi size (right) in *Atf2*$^{WT/WT}$ (n = 9) and *Atf2*$^{\Delta 8,9/\Delta 8,9}$ mice (n = 8) on a *Braf*$^{WT/WT}$ background, 250 days following perinatal 4-HT administration. The data are the mean ± SEM (p value was calculated by two-tailed unpaired t test).

(legend continued on next page)

Importantly, we also assessed the possible importance of ATF2^{SV5} expression in human melanoma tumors. The relative expression of ATF2^{SV5} and ATF2^{WT} / ATF2^{SV3} were measured in 33 melanoma tumor specimens that were obtained from 21 consenting metastatic melanoma patients at the time of tumor resection or upon autopsy. A total of 18 (54.5%) of the biopsies came from autopsy samples. Notably, a higher level of ATF2^{SV5} (>3-fold) was found to coincide with poorer prognosis (Figure 4K). Of the top 11 highest ATF2^{SV5} expressing tumors (quantification cycle (cq) < 33.5), seven (63.6%) were from tumor biopsies obtained shortly after death and four (36.4%) were from patients who were double BRAF/NRAS wild-type. These observations substantiate the findings made in the genetic mouse model as in the cultured melanoma and melanocytes, where transcriptionally inactive ATF2 variants elicit a gain of function oncogenic activity.

DISCUSSION

We identified an unexpected role for transcriptionally inactive ATF2 in melanocyte homeostasis and melanoma development. *Atf2*$^{\Delta 8,9}$ alone is able to drive the formation of nevi within 2–3 months and induction of the melanomagenesis. When combined with the *Braf* mutant genotype, *Atf2*$^{\Delta 8,9}$ was able to drive the development of melanoma over 250 days. These animals also exhibit upregulation of select gene networks, including pigmentation-related genes, chemokines/cytokines implicated in the recruitment of immune cells to the tumor sites, and genes related to the enhanced propensity for metastasis. Further, *Atf2*$^{\Delta 8,9}$ accelerated the formation of melanomas and increased their propensity to metastasize in *Braf*/*Pten* mutant animals. These data establish the ability of a transcriptionally inactive form of ATF2 to promote *Braf*^{V600E} melanoma development and progression.

Although *Atf2*$^{\Delta 8,9}$ enhanced the pigmentation program in both Nras and Braf mutant melanocytes, it attenuated melanoma development in *Nras* mutant mice and enhanced it in *Braf* mutant mice. These differences may be attributed to an effect of *Atf2*$^{\Delta 8,9}$ on specific signaling pathways that cooperate with *Braf*, but not *Nras*, and/or to its effect on tumor microenvironment (i.e., immune editing; tumor stroma).

While full-length transcriptionally active ATF2 is largely oncogenic in melanoma, its transcriptionally inactive splice variants, represented by human ATF2^{SV5} and modeled by mouse ATF2$^{\Delta 8,9}$, exhibit a super-oncogenic function. Genes that were commonly deregulated by expression of both human and mouse variants (ATF2^{SV5} and ATF2$^{\Delta 8,9}$, respectively) were primarily implicated in metastasis (CCL4, CCR7, S100A8, and MITF), immune cell infiltration (CCL4, CCR7, and TIM3), and melanoma progression / drug resistance (MITF).

Expression of ATF2^{SV5} in a series of 33 melanoma biopsies coincides with poor prognosis, consistent with our findings in ATF2$^{\Delta 8,9}$ mouse melanoma models. Notably, although the activity of ATF2^{SV5} is expected to supersede that of other ATF2 forms, it is co-expressed with other ATF2 forms (full-length and other splice variants).

Collectively, our studies provide a genetic support for the involvement of a gain-of-function ATF2 isoform in melanoma. Our data demonstrate that the transcriptionally inactive variant is able to drive melanomagenesis and, in cooperation with mutant *Braf*, induce melanoma development at the slow rate often seen in human melanoma. Our findings highlight the importance of ATF2 function also as a transcriptionally inactive form.

EXPERIMENTAL PROCEDURES

For additional experimental procedures, see Supplemental Experimental Procedures.

Animal Studies and In Vivo Experiments

All animal studies were approved by the Institutional Animal Care and Use Committee of the Sanford Burnham Prebys Medical Discovery Institute. *Atf2*$^{\Delta 8,9/\Delta 8,9}$ mice, described in earlier studies (Shah et al., 2010), were crossed with *Braf*$^{V600E/V600E}$;*Pten*$^{-/-}$ mice (Dankort et al., 2009). *Atf2*$^{\Delta 8,9/\Delta 8,9}$ and *Atf2*$^{\Delta 8,9/\Delta 8,9}$;*Braf*$^{WT/V600E}$ are C57BL/6 and *Atf2*$^{\Delta 8,9/\Delta 8,9}$;*Braf*$^{V600E/V600E}$;*Pten*$^{-/-}$ are C57BL/6 × 129.

Activation of the *Tyr::CreER*^{T2} Transgene

Topical administration of 4-HT (Sigma-Aldrich) was performed by application of 10 μl of a 50 mg/ml solution in DMSO with a paintbrush onto the dorsal skin of pups on days 1, 3, and 5 after birth. Local administration of 4-HT was performed by application of 1.5 μl of a 7.8 mg/ml solution in ethanol onto the shaved dorsal skin of 3-week-old mice (Scortegagna et al., 2014).

Cell Lines

The YUMM1.3 cell line was generated from a *Braf*$^{WT/V600E}$;*Pten*$^{-/-}$;*Cdkn2a*$^{-/-}$ melanoma in C57BL/6 mice (Scortegagna et al., 2015). The human UACC91,

(B) Tumor weights of *Atf2*$^{\Delta 8,9/WT}$ (n = 14), *Atf2*$^{WT/WT}$ (n = 16), and *Atf2*$^{\Delta 8,9/\Delta 8,9}$ (n = 18) mice on a *Braf*$^{WT/V600E}$ background, 250 days following systemic 4-HT administration. The proportion of *Atf2*$^{\Delta 8,9/WT}$, *Atf2*$^{\Delta 8,9/\Delta 8,9}$, and *Atf2*$^{WT/WT}$ mice developing tumors was 28%, 50%, and 0%, respectively. The data are the mean ± SEM (p value was calculated by two-tailed unpaired t test).

(C and D) H&E analysis of skin (C) and S100 immunostaining of tumors (D) from *Atf2*$^{WT/WT}$ and *Atf2*$^{\Delta 8,9/\Delta 8,9}$ mice on a *Braf*$^{WT/V600E}$ background. Samples were analyzed at the time of collection. The scale bars represent 300 μm.

(E and F) Colony forming assay (E) and migration assay (F) of human H3A melanocytes transduced with control (Scr) or with vectors expressing shATF2 (targeting ATF2^{WT} and ATF2^{SV3}, but not ATF2^{SV5}) ATF2^{WT}, ATF2^{SV3}, ATF2^{SV5}, or ATF2$^{\Delta 8,9}$. The data are the mean ± SEM (p value was calculated by two-tailed unpaired t test).

(G and H) Colony forming assays of H3A cells generated as described for (E) and (F) and additionally transduced with BRAF^{V600E} (G) or NRAS^{Q61K} (H). The data are the mean ± SEM (p value was calculated by two-tailed unpaired t test).

(I) Migration of H3A cells transfected with control siRNA or siRNA targeting ATF2^{WT} and ATF2^{SV3} or targeting ATF2^{SV5} alone. The data are the mean ± SEM (p value was calculated by two-tailed unpaired t test).

(J) qPCR analysis of human melanoma C054 and LU1205 cell lines subjected to KD of ATF2^{WT} and ATF2^{SV3} (ATF2$^{WT/SV3}$) or ATF2^{SV5}. The genes analyzed were upregulated in *Atf2*$^{\Delta 8,9/\Delta 8,9}$;*Braf*$^{V600E/V600E}$;*Pten*$^{-/-}$ mice (see also Figure S2D). Lu1205 do not express *SILVER* and *MELAN-A*. qPCR values are normalized to the expression levels in cells transfected with a control siRNA. The data are the mean ± SEM.

(K) qPCR analysis of relative transcript levels of *ATF2*^{WT} and *ATF2*^{SV3} or *ATF2*^{SV5} in 33 melanoma specimens from 21 patients. See also Figure S4 and Tables S3 and S4. The data are the mean ± SEM.

UACC2427, and UACC1113 cell lines were kindly provided by Drs. Brown and Lin. H3A immortalized melanocyte cells were provided by Dr. Bennet (Gray-Schopfer et al., 2006). All cell lines except H3A were maintained in DMEM supplemented with 10% fetal bovine serum (FBS) and 1% penicillin and streptomycin. H3A cell lines were propagated in 254 media (Gibco) and transferred to DMEM medium prior to initiating the experiments.

Statistical Analysis

Data are presented as means ± SEM or SD and the statistical significance (p value) was determined by two-tailed unpaired t test. Kaplan-Meyer survival curves were compiled using Prism statistical analysis software and significance was assessed using the log rank (Mantel-Cox) test. A p value of < 0.05 was considered significant.

ACCESSION NUMBERS

Microarray datasets were deposited in the NCBI GEO database under GEO: GSE79917 and GSE81014.

SUPPLEMENTAL INFORMATION

Supplemental Information includes Supplemental Experimental Procedures, four figures, and four tables and can be found with this article online at http://dx.doi.org/10.1016/j.celrep.2016.04.072.

AUTHOR CONTRIBUTIONS

G.C., H.K., M.S., and Z.A.R. designed experiments; G.C. and Y.C. performed experiments; A.D., N.K.H., and M.B. provided reagents/samples; G.C., Y.C., M.S., H.K., E.L., J.Q., B.J., T.Z., J.-L.L., M.P.L., R.D., M.B., K.M.B., and Z.A.R. analyzed data; and G.C. and Z.A.R. wrote the manuscript.

ACKNOWLEDGMENTS

We thank Drs. N. Jones and W. Breitweiser for sharing the ATF2 mutant mouse model; M. McMahon, M. Soengas, D. Bennet, and H. Yin for plasmids and cell lines; R. Newlin, G. Garcia, J. Morales, and V. Ylis for technical assistance in histology and animal work; and members of the Z.A.R. laboratory for helpful discussions. Core Services were supported by NCI Cancer Center Support Grant P30 CA30199. T.Z. and K.M.B. were supported by the Division of Cancer Epidemiology and Genetics at NCI. We thank the biobank of the University Research Priority Program (URPP) in translational cancer research for biopsy materials. This work utilized the computational resources of the NIH HPC Biowulf cluster (https://hpc.nih.gov). N.K.H. was supported by a fellowship from the National Health and Medical Research Council of Australia. G.C. was also supported by a Research Scholar Award from the Joanna M. Nicolay Melanoma Foundation. Support from NCI grants CA99961 and CA172017, the Melanoma Research Foundation, and the Hervey Family Non-endowment Fund at The San Diego Foundation to Z.A.R. is gratefully acknowledged.

Received: September 16, 2015
Revised: March 15, 2016
Accepted: April 19, 2016
Published: May 19, 2016

REFERENCES

Balch, C.M., Gershenwald, J.E., Soong, S.J., Thompson, J.F., Atkins, M.B., Byrd, D.R., Buzaid, A.C., Cochran, A.J., Coit, D.G., Ding, S., et al. (2009). Final version of 2009 AJCC melanoma staging and classification. J. Clin. Oncol. *27*, 6199–6206.

Berger, A.J., Kluger, H.M., Li, N., Kielhorn, E., Halaban, R., Ronai, Z., and Rimm, D.L. (2003). Subcellular localization of activating transcription factor 2 in melanoma specimens predicts patient survival. Cancer Res. *63*, 8103–8107.

Bhoumik, A., Huang, T.G., Ivanov, V., Gangi, L., Qiao, R.F., Woo, S.L., Chen, S.H., and Ronai, Z. (2002). An ATF2-derived peptide sensitizes melanomas to apoptosis and inhibits their growth and metastasis. J. Clin. Invest. *110*, 643–650.

Bhoumik, A., Gangi, L., and Ronai, Z. (2004a). Inhibition of melanoma growth and metastasis by ATF2-derived peptides. Cancer Res. *64*, 8222–8230.

Bhoumik, A., Jones, N., and Ronai, Z. (2004b). Transcriptional switch by activating transcription factor 2-derived peptide sensitizes melanoma cells to apoptosis and inhibits their tumorigenicity. Proc. Natl. Acad. Sci. USA *101*, 4222–4227.

Bhoumik, A., Fichtman, B., Derossi, C., Breitwieser, W., Kluger, H.M., Davis, S., Subtil, A., Meltzer, P., Krajewski, S., Jones, N., and Ronai, Z. (2008). Suppressor role of activating transcription factor 2 (ATF2) in skin cancer. Proc. Natl. Acad. Sci. USA *105*, 1674–1679.

Breitwieser, W., Lyons, S., Flenniken, A.M., Ashton, G., Bruder, G., Willington, M., Lacaud, G., Kouskoff, V., and Jones, N. (2007). Feedback regulation of p38 activity via ATF2 is essential for survival of embryonic liver cells. Genes Dev. *21*, 2069–2082.

Dankort, D., Curley, D.P., Cartlidge, R.A., Nelson, B., Karnezis, A.N., Damsky, W.E., Jr., You, M.J., DePinho, R.A., McMahon, M., and Bosenberg, M. (2009). Braf(V600E) cooperates with Pten loss to induce metastatic melanoma. Nat. Genet. *41*, 544–552.

Dutton-Regester, K., Irwin, D., Hunt, P., Aoude, L.G., Tembe, V., Pupo, G.M., Lanagan, C., Carter, C.D., O'Connor, L., O'Rourke, M., et al. (2012). A high-throughput panel for identifying clinically relevant mutation profiles in melanoma. Mol. Cancer Ther. *11*, 888–897.

Gozdecka, M., Lyons, S., Kondo, S., Taylor, J., Li, Y., Walczynski, J., Thiel, G., Breitwieser, W., and Jones, N. (2014). JNK suppresses tumor formation via a gene-expression program mediated by ATF2. Cell Rep. *9*, 1361–1374.

Gray-Schopfer, V.C., Cheong, S.C., Chong, H., Chow, J., Moss, T., Abdel-Malek, Z.A., Marais, R., Wynford-Thomas, D., and Bennett, D.C. (2006). Cellular senescence in naevi and immortalisation in melanoma: a role for p16? Br. J. Cancer *95*, 496–505.

Katz, Y., Wang, E.T., Airoldi, E.M., and Burge, C.B. (2010). Analysis and design of RNA sequencing experiments for identifying isoform regulation. Nat. Methods *7*, 1009–1015.

Lau, E., and Ronai, Z.A. (2012). ATF2 - at the crossroad of nuclear and cytosolic functions. J. Cell Sci. *125*, 2815–2824.

Lau, E., Kluger, H., Varsano, T., Lee, K., Scheffler, I., Rimm, D.L., Ideker, T., and Ronai, Z.A. (2012). PKCε promotes oncogenic functions of ATF2 in the nucleus while blocking its apoptotic function at mitochondria. Cell *148*, 543–555.

Lo, J.A., and Fisher, D.E. (2014). The melanoma revolution: from UV carcinogenesis to a new era in therapeutics. Science *346*, 945–949.

Lopez-Bergami, P., Lau, E., and Ronai, Z. (2010). Emerging roles of ATF2 and the dynamic AP1 network in cancer. Nat. Rev. Cancer *10*, 65–76.

Maekawa, T., Sano, Y., Shinagawa, T., Rahman, Z., Sakuma, T., Nomura, S., Licht, J.D., and Ishii, S. (2008). ATF-2 controls transcription of Maspin and GADD45 alpha genes independently from p53 to suppress mammary tumors. Oncogene *27*, 1045–1054.

Scortegagna, M., Ruller, C., Feng, Y., Lazova, R., Kluger, H., Li, J.L., De, S.K., Rickert, R., Pellecchia, M., Bosenberg, M., and Ronai, Z.A. (2014). Genetic inactivation or pharmacological inhibition of Pdk1 delays development and inhibits metastasis of Braf(V600E):Pten(-/-) melanoma. Oncogene *33*, 4330–4339.

Scortegagna, M., Lau, E., Zhang, T., Feng, Y., Sereduk, C., Yin, H., De, S.K., Meeth, K., Platt, J.T., Langdon, C.G., et al. (2015). PDK1 and SGK3 contribute to the growth of BRAF-mutant melanomas and are potential therapeutic targets. Cancer Res. *75*, 1399–1412.

Shah, M., Bhoumik, A., Goel, V., Dewing, A., Breitwieser, W., Kluger, H., Krajewski, S., Krajewska, M., Dehart, J., Lau, E., et al. (2010). A role for ATF2 in regulating MITF and melanoma development. PLoS Genet. *6*, e1001258.

Wang, E.T., Sandberg, R., Luo, S., Khrebtukova, I., Zhang, L., Mayr, C., Kingsmore, S.F., Schroth, G.P., and Burge, C.B. (2008). Alternative isoform regulation in human tissue transcriptomes. Nature *456*, 470–476.